



The influence of reaction temperature on the chemical structure and surface concentration of active NO_x in H₂-SCR over Pt/MgO–CeO₂: SSITKA-DRIFTS and transient mass spectrometry studies

Petros G. Savva, Angelos M. Efstathiou*

Chemistry Department, Heterogeneous Catalysis Laboratory, University of Cyprus, P.O. Box 20537, CY 1678, Nicosia, Cyprus

ARTICLE INFO

Article history:

Received 12 January 2008

Revised 26 March 2008

Accepted 11 May 2008

Available online 12 June 2008

Keywords:

Lean de-NO_x

H₂-SCR

NO reduction

SSITKA-DRIFTS

Transient experiments

H spillover

ABSTRACT

Steady-state isotopic transient kinetic analysis (SSITKA), transient isothermal, and temperature-programmed surface reaction in H₂ (H₂-TPSR) techniques coupled with online mass spectroscopy (MS) and in situ diffuse reflectance infrared Fourier transform spectroscopy (DRIFTS) were used to study essential mechanistic and kinetic aspects of the selective catalytic reduction (SCR) of NO with the use of H₂ under strongly oxidizing conditions (H₂-SCR) over a novel Pt/MgO–CeO₂ catalyst. The main focus was to study and report for the first time the effects of reaction temperature on the *chemical structure* and *surface concentration* of the active NO_x intermediate species thereby formed. The information obtained is essential to understanding the volcano-type profile of the catalyst activity versus reaction temperature observed here and also reported previously. In the present work, two active NO_x intermediate species identified by SSITKA-DRIFTS were found in the nitrogen-reaction path toward N₂ and N₂O formation, one species located in the vicinity of the Pt–CeO₂ support interface region (nitrosyl [NO⁺] coadsorbed with a nitrate [NO₃⁻] species on an adjacent Ce⁴⁺–O²⁻ site pair) and the second located in the vicinity of the Pt–MgO support interface region. The chemical structure of the second kind of active NO_x species was found to depend on reaction temperature. In particular, the chemical structure was that of bidentate or monodentate nitrate (NO₃⁻) at *T* < 200 °C and that of chelating nitrite (NO₂⁻) at *T* > 200 °C. The concentration of the active NO_x intermediates that lead to N₂ formation was found to be practically independent of reaction temperature (120–300 °C) and significantly larger than 1 equivalent monolayer of surface Pt ($\theta_{\text{NO}_x} = 2.4\text{--}2.6$). The former result cannot be used to explain the volcano-type behavior of the catalytic activity versus the reaction temperature observed; alternative explanations are explored. The H-spillover process involved in the H₂-SCR mechanism was found to be limited within a support region of about a 4–5 Å radius around the Pt nanoparticles ($d_{\text{Pt}} = 1.2\text{--}1.5$ nm).

© 2008 Elsevier Inc. All rights reserved.

1. Introduction

Selective catalytic reduction (SCR) of NO_x from an industrial flue gas stream at low temperature (*T* < 200 °C) has many advantages over that at higher temperature (*T* > 350 °C); for example, placement of the catalyst after the electrostatic precipitator unit implies that the partially cleaned flue gas from dust requires less soot blowing and catalyst cleaning, thus providing longer catalyst lifetime. Furthermore, the low-temperature SCR process can reduce both investment and operating costs for two reasons. First, the SCR unit can be located at the end of the stack gas train (low-temperature region), thus minimizing the need to run ductwork from a high-temperature region and then return the flue gas to the stack gas train. Second, much less reheating of the flue gas from

the de-SO_x to the SCR unit is required [1–4]. New low-temperature SCR catalysts also are capable of retrofitting large utility boilers and installations firing natural gas or refinery fuel gas.

Successful industrial low-temperature SCR catalysts must be active and stable in the presence of H₂O, CO₂, and SO₂ in the flue gas stream, the composition of which depends on the fuel used. Low-temperature NH₃-SCR catalysts (180–240 °C) are currently used in some industrial applications [5–7]; however, besides the general problems associated with NH₃-SCR NO_x control technology (stationary applications) [2,8,9], the main disadvantage of the low-temperature NH₃-SCR catalyst is its susceptibility to ammonium bisulphate precipitation and to fouling by solid particulates.

Apart from the aforementioned problems faced by the current NH₃-SCR NO_x control technology, which necessitate the urgent development of new SCR catalysts, the use of green technologies to lead to the simultaneous reduction of both CO₂ and NO_x emissions demands new noncarbon-containing reducing agents for the catalytic elimination of NO_x from industrial flue gas streams at low

* Corresponding author. Fax: +357 22 892801.

E-mail address: efstath@ucy.ac.cy (A.M. Efstathiou).

temperature ($T < 200\text{ }^{\circ}\text{C}$) while also reducing investment and operating costs.

Recent research from our laboratory [10–15] has demonstrated that industrial H_2 -SCR of NO at 120–160 $^{\circ}\text{C}$ is possible over a novel Pt/MgO–CeO₂ catalyst [15]. Until the complete transition to a hydrogen economy and zero greenhouse gas emissions are achieved, H_2 -SCR may be considered as a breakthrough NO_x control technology over the currently used NH₃-SCR approach.

In the present work, for the first time the effects of reaction temperature on the chemical structure and surface concentration of active and inactive (spectator) NO_x intermediate species in the H_2 -SCR of NO under working reaction conditions at 120–300 $^{\circ}\text{C}$ were determined by SSITKA-DRIFTS, SSITKA-MS, transient isothermal, and temperature-programmed surface reaction in H_2 (H_2 -TPSR) experiments performed over the novel 0.1 wt% Pt/MgO–CeO₂ catalyst. The results provide insight into the volcano-type profile of reaction rate and NO conversion versus reaction temperature (X_{NO} vs T) observed here and also reported previously [13,14].

2. Experimental

2.1. Catalyst preparation and characterization

The catalyst support, comprising 50 wt% MgO and 50 wt% CeO₂, was prepared by the sol-gel method as described previously [14, 16]. Mg(EtO)₂ (Aldrich) and Ce(NO₃)₃·H₂O (Aldrich) were used as precursors of Mg and Ce, respectively. The 0.1 wt% Pt/MgO–CeO₂ catalyst was prepared by the incipient wetness impregnation method, using H₂Pt(IV)Cl₆ (Aldrich) as a metal precursor. After water evaporation and drying overnight at 120 $^{\circ}\text{C}$, the solid residue was ground and calcined in air at 600 $^{\circ}\text{C}$ for 2 h. The fresh catalyst sample was pretreated in situ in 5%O₂/He at 600 $^{\circ}\text{C}$ for 2 h and then reduced in 10%H₂/He at 300 $^{\circ}\text{C}$ for 2 h before any experiments.

H₂ chemisorption at 25 $^{\circ}\text{C}$, followed by TPD, and HRTEM were used to measure Pt dispersion and particle size over the 0.1 wt% Pt/MgO–CeO₂ catalyst [13]. The dispersion of Pt was found to be about 90%, with an estimated mean Pt particle size of 1.2–1.5 nm. XRD studies revealed primary crystal sizes (using Scherrer's equation) of 10 nm for MgO and 12 nm for CeO₂, whereas SEM studies revealed a wide range of secondary particle size (1–10 μm) for the MgO and CeO₂ solid phases [17].

2.2. Transient mass spectrometry studies

The SSITKA and H_2 -TPSR experiments were performed in a specially designed transient gas flow system using a quartz microreactor [18–20]. The amount of catalyst (Pt/MgO–CeO₂) used in the SSITKA experiments was varied so as to keep the NO conversion below 15% in the entire temperature range investigated (120–300 $^{\circ}\text{C}$). The total amount of catalytic bed material was 0.15 g in all SSITKA experiments after the active catalytic component was diluted with silica. The total flow rate was kept constant at 30 NmL/min. An online quadrupole mass spectrometer (Omnistar, Balzers) was used for the chemical analysis of the gas effluent stream from the reactor. Standard gas mixtures were used to calibrate the signals obtained by the mass spectrometer.

Table 1 describes the necessary sequence of step changes in gas composition performed for the SSITKA and H_2 -TPSR experiments. The reaction mixture of H_2 -SCR consisted of 0.25 vol% NO, 1 vol% H₂, 5 vol% O₂, and the balance He. The SSITKA experiments involved the switching of ¹⁴NO/H₂/O₂/Ar/He to the equivalent isotopic ¹⁵NO/H₂/O₂/He gas mixture after steady state was achieved. The Ar gas was used as a tracer; its decay was used to monitor the system's gas-phase holdup [20]. After the switch of ¹⁴NO/H₂/O₂/Ar/He → ¹⁵NO/H₂/O₂/He, the following mass numbers

Table 1

Sequential step changes of feed gas composition during transient isotopic and H_2 -TPSR experiments

Experiment code	Sequence of step changes of gas flow
A	¹⁴ NO/H ₂ /O ₂ /Ar/He (30 min, T) → ¹⁵ NO/H ₂ /O ₂ /He (t, T) (SSITKA)
B	¹⁴ NO/H ₂ /O ₂ /Ar/He (30 min, T) → ¹⁵ NO/He (15 min, T) → cool quickly to room T in ¹⁵ NO/He → He (5 min) → H_2 -TPSR (10%H ₂ /He)

(m/z) were continuously monitored: 2 for H₂, 28 for ¹⁴N₂, 29 for ¹⁴N¹⁵N, 30 for ¹⁴NO, 31 for ¹⁵NO, 32 for O₂, 40 for Ar, 44 for ¹⁴N₂O, and 45 for ¹⁴N¹⁵NO. Details of the mass spectrometry analysis of the reactor gas effluent stream have been reported previously [11, 21]. Note that under the present reaction conditions for H_2 -SCR of NO, neither NH₃ nor NO₂ gas products were formed. A 1.0 vol% ¹⁵NO/He gas mixture (ISOTEC, Inc.) was used in all SSITKA and other transient isotopic experiments.

2.3. Transient DRIFTS studies

DRIFTS spectra were recorded on a Perkin-Elmer GX II FTIR spectrophotometer at a resolution of 2 cm⁻¹ coupled with a high-temperature/high-pressure controllable DRIFTS cell (Harrick Scientific) equipped with ZnSe IR windows. About 30 mg of solid catalyst (Pt/MgO–CeO₂) in powder form was used in each experiment, with the total flow rate kept constant at 50 NmL/min. Under these conditions, the conversion of NO was kept below 15% during the SSITKA-DRIFTS experiments. Before all DRIFTS experiments, the Pt-supported catalyst was pretreated in 5%O₂/Ar for 2 h at 600 $^{\circ}\text{C}$, then in a 10%H₂/Ar gas mixture at 300 $^{\circ}\text{C}$ for 2 h. The feed was then switched to pure Ar for 15 min at 300 $^{\circ}\text{C}$, after which the sample was cooled to the appropriate temperature for the subsequent experiment. For FTIR single-beam background subtraction, the IR spectrum of the solid was obtained in Ar flow at the appropriate temperature. DRIFTS spectra were collected at the rate of 1 scan/s in the 3000–800 cm⁻¹ range. The average spectrum (30 spectra were collected) was then analyzed using the instrument's Spectrum for Windows software along with deconvolution and curve-fitting procedures suggested in the literature [22]. The various IR absorption bands due to adsorbed NO_x species were assigned based on the literature and similar SSITKA-DRIFTS studies performed on the 0.1 wt% Pt/MgO and 0.1 wt% Pt/CeO₂ catalysts [21,23–32].

3. Results and discussion

3.1. In situ DRIFTS studies

3.1.1. Chemical structure of active and inactive adsorbed NO_x—SSITKA experiments

The chemical structure of the active NO_x species that truly participate in the nitrogen reaction path of the H_2 -SCR of NO as a function of reaction temperature in the 120–300 $^{\circ}\text{C}$ range was studied by SSITKA experiments in the DRIFTS cell, which was operated as a differential microreactor. DRIFTS spectra were first recorded after 30 min of reaction in the ¹⁴NO/H₂/O₂ gas mixture. The reaction feed stream was then switched to the equivalent isotopic ¹⁵NO/H₂/O₂ gas mixture (experiment A in Table 1), and DRIFTS spectra were recorded after 30 min of reaction (new steady state). Figs. 1a and 1b show DRIFTS spectra recorded in the 2400–1100 cm⁻¹ range over the 0.1 wt% Pt/MgO–CeO₂ catalyst at 120 and 300 $^{\circ}\text{C}$, respectively, under the nonisotopic and isotopic gas mixtures. It can be seen that the shape and position of several IR bands have changed under the ¹⁵NO isotopic gas mixture. Table 2 reports the chemical structure and the corresponding absorption IR

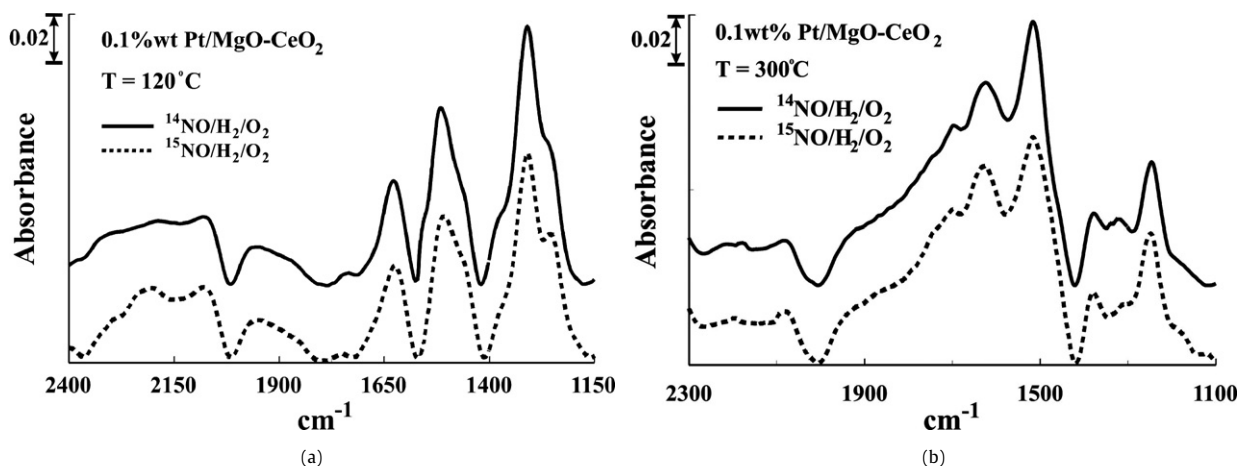
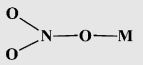
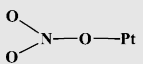
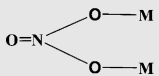
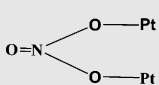
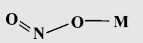
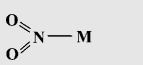
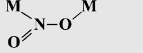
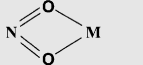
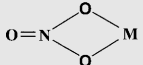
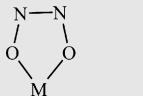


Fig. 1. In situ SSITKA-DRIFTS spectra recorded after 30 min of $^{14}\text{NO}/\text{H}_2/\text{O}_2/\text{Ar}$ reaction (—) (H_2 -SCR) and after 30 min of the isotopic switch to $^{15}\text{NO}/\text{H}_2/\text{O}_2/\text{Ar}$ (---) over the 0.1 wt% Pt/MgO-CeO₂ catalyst at (a) 120 °C and (b) 300 °C. Feed composition: $\text{H}_2 = 1.0$ vol%, $\text{NO} = 0.25$ vol%, $\text{O}_2 = 5$ vol%, and Ar as balance gas.

Table 2

Chemical structures and absorption IR bands (stretching modes) of various adsorbed NO_x species on metal oxide-supported Pt catalysts [21,23–32]

Species	Structure	Vibration	Wavenumber (cm ⁻¹)
Nitric oxide	NO(g)	$\nu(\text{NO})$	1883
Nitrogen hypoxide	M-N ₂ O	$\nu(\text{NO})$	2224
		$\nu(\text{NN})$	1286
Nitrosyls on metal oxide support	M-NO ⁺	$\nu(\text{NO})$	2220
	M-NO ₂ ⁺	$\nu(\text{NO}_2,a)$	2360–2375
		$\nu(\text{NO}_2,s)$	1400
Nitrosyls on Pt	M-NO ₂ ^{δ+} , M-NO ^{δ+}		2100–2200
	NO-Pt _{ox}	$\nu(\text{NO})$	~1840
	NO-Pt _{red}	$\nu(\text{NO})$	~1800
	NO ^{δ+} -Pt	$\nu(\text{NO})$	1900–2000
Bridged or bent NO on Pt	Pt _n -NO	$\nu(\text{NO})$	1500–1700 (depending on n)
Monodentate nitrates		$\nu(\text{NO}_2,a)$	1450–1570
		$\nu(\text{NO}_2,s)$	1250–1330
		$\nu(\text{NO})$	970–1035
			1620–1660
Bridged nitrates		$\nu(\text{NO}_2,a)$	1170–1300
		$\nu(\text{NO}_2,s)$	1000–1030
		$\nu(\text{NO})$	1590–1660
			1520–1610
Nitrites		$\nu(\text{N=O})$	1400–1485
		$\nu(\text{NO})$	1050–1110
		$\nu(\text{ONO})$	820–850
Nitrito complex		$\nu(\text{NO}_2,a)$	1335–1470
		$\nu(\text{NO}_2,s)$	1315–1350
		$\nu(\text{ONO})$	820–850
Bridging nitro complex		$\nu(\text{NO}_2,a)$	1390–1520
		$\nu(\text{NO}_2,s)$	1180–1260
Chelating nitrite (NO ₂ ⁻)		$\nu(\text{NO}_2,a)$	1260–1390
		$\nu(\text{NO}_2,s)$	1170–1210
		$\nu(\text{ONO})$	840–860
Bidentate nitrate		$\nu(\text{NO}_2,a)$	1200–1310
		$\nu(\text{NO}_2,s)$	1003–1040
		$\nu(\text{N=O})$	1500–1620
Dimeric NO, N ₂ O ₂ ²⁻		$\nu(\text{NO})$	1383
		$\nu(\text{NN})$	1115

M = metal cation of metal oxide.

bands (stretching modes) of various adsorbed NO_x species, many of which were observed in the present work and reported in well-documented experimental and theoretical studies [21,23–32].

After appropriate deconvolution [22] of the spectral region shown in Fig. 1a ($T = 120$ °C), it was found that three IR bands gave a red isotopic shift. The results are presented in Figs. 2a–2c. The figure shows only spectra deconvolution and curve fitting associated with the $^{14}\text{NO}/\text{H}_2/\text{O}_2$ reaction, along with the IR band that gave the red isotopic shift under the $^{15}\text{NO}/\text{H}_2/\text{O}_2$ reaction conditions (dashed line after the deconvolution and curve-fitting procedures). The IR bands that shifted to lower wavenumbers under the isotopic switch correspond to *active* adsorbed NO_x intermediates formed during the $^{14}\text{NO}/\text{H}_2/\text{O}_2$ reaction that eventually led to N₂ and N₂O, whereas those that did not give the red isotopic shift correspond to *inactive* (spectator) adsorbed NO_x species. The possibility of having an exchangeable adsorbed $^{14}\text{NO}_x$ species with gaseous ^{15}NO that may not be an active reaction intermediate has been studied previously [21,26]; however, in some cases, making clear assignments for the true structure of active NO_x present on the metal oxide support surface is not possible, for several reasons:

- Similar IR bands appear in more than one kinds of NO_x in the 2300–1000 cm⁻¹ region, where the contribution of metal oxide support at frequencies below 1000 cm⁻¹ is not negligible; for example, two vibrational modes of unidentate (ν_{as} , ν_s) and bidentate (ν_a , N=O) nitrates give rise to very similar IR bands (see Table 2).
- Similarly structured NO_x species can appear as either active or inactive adsorbed species during the H₂-SCR of NO ($^{14}\text{NO}/\text{H}_2/\text{O}_2$) (same IR band) on the present Pt/MgO-CeO₂ catalyst according to DRIFTS experiments described and discussed in Section 3.1.2, a result that does not allow estimation of the relative intensities of the vibrational modes of similarly structured NO_x species (the case of nitrates and nitrites; Table 2), which could overcome the difficulty noted in (a). For example, Fig. 2a shows two IR bands centered at 1250 cm⁻¹, one band associated with active NO_x (red isotopic shift) and the other associated with inactive NO_x of the same structure.

Despite these difficulties, however, our SSITKA-DRIFTS results allow us to demonstrate the true location of the active NO_x species—for example, whether they are formed on the metal (Pt) or the support surface. This important result is strongly supported by the SSITKA-MS studies (see Section 3.2), allowing for the quantification of the true active NO_x intermediate species. The concentration of the latter species was found to be largely in excess of a monolayer based on the exposed Pt metal surface.

Considering the aforementioned findings, the observed shift from 1250 to 1210 cm⁻¹ (Fig. 2a) can be assigned to the asymmet-

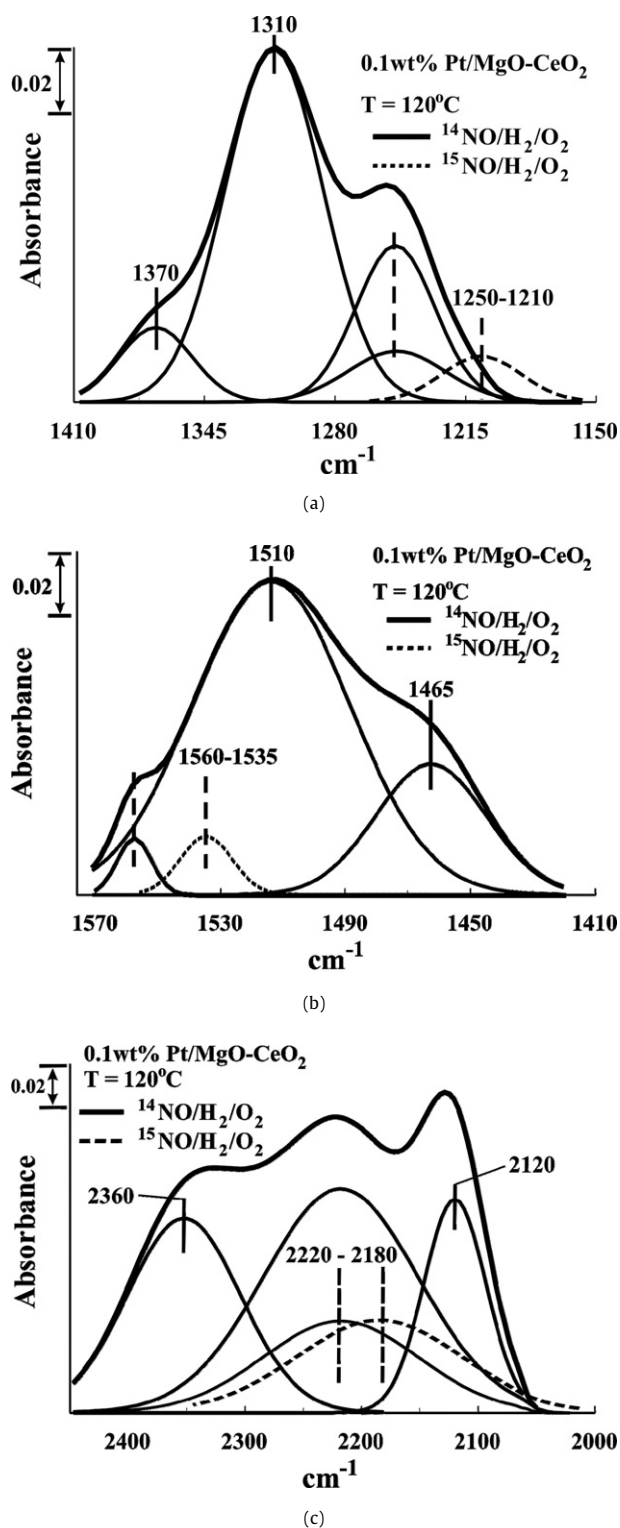


Fig. 2. Deconvolution and curve fitting of SSITKA-DRIFTS spectra recorded at 120°C in the H₂-SCR of NO over 0.1 wt% Pt/MgO–CeO₂ catalyst in the spectral region (a) 1410–1150 cm⁻¹, (b) 1570–1410 cm⁻¹, and (c) 2450–2000 cm⁻¹.

ric or the symmetric vibrational mode of bidentate or monodentate nitrate formed on the MgO support, as discussed previously [21]. In that study (Fig. 5, Ref. [21]), a similar SSITKA-DRIFTS experiment as that shown in Fig. 2 was performed on 0.1 wt% Pt/MgO and 0.1 wt% Pt/CeO₂ catalysts, with the observed isotopic shifts assigned to different active adsorbed NO_x species based on the results of Table 2.

In Fig. 2b, the observed shift from 1560 to 1535 cm⁻¹ is assigned to the N–O stretching vibrational mode of bidentate nitrate or the asymmetric mode of monodentate nitrate (see Table 2), the same NO_x species giving the red isotopic shift from 1250 to 1210 cm⁻¹ shown in Fig. 2a. The results of Figs. 2a and 2b indicate the accuracy of the spectral analysis, illustrating that all vibrational modes of a given NO_x adsorbed species assumed to be active are expected to give the red isotopic shift. Separation of the aforementioned two IR nitrate bands was found to increase with bidentate nitrates compared with monodentate nitrates [33]. Machida et al. [34] reported an observable experimental difference of 340 versus 250 cm⁻¹ for the two IR bands due to nitrates on the Pt/TiO₂–ZrO₂ catalyst during NO/H₂/O₂ reaction at 90°C, which were assigned to bidentate and unidentate nitrates, respectively. In the present work (Figs. 2a and 2b), the observed difference was 310 cm⁻¹, which could favor the assignment to a bidentate nitrate species.

There is a discussion in the literature [24] about the nature of NO_x species observed in the 2300–2100 cm⁻¹ range. The N₂O(g) molecular species has a stretching N–N vibrational mode at 2224 cm⁻¹, practically the same as that shown in Fig. 2c. Previously, we reported that under the present experimental conditions and in the DRIFTS cell used, it was impossible for this IR band to be due to gaseous N₂O [21]. Furthermore, we report here that the isotopic shift for the N–N bond would be expected to be ~75 cm⁻¹ [24], as opposed to the observed shift of about 40 cm⁻¹ (Fig. 2c). NO⁺ and NO₂⁺ adsorbed species on metal oxide surfaces also gave IR bands in the 2200–2100 cm⁻¹ range. In the present work, the observed IR band shift from 2220 to 2180 cm⁻¹ (Fig. 2c) is assigned to nitrosyl (NO⁺) coadsorbed with a nitrate (NO₃⁻) species on adjacent metal cation–oxygen anion site pair of the CeO₂ support surface, as we discussed in previous work [21]. The main reasoning for this is as follows:

- Similar SSITKA-DRIFTS experiments were performed on 0.1 wt% Pt/MgO and 0.1 wt% Pt/CeO₂ catalysts, where only for the latter catalyst a red isotopic shift from 2220 to 2190 was observed.
- A TPSR in H₂/He experiment, following H₂-SCR of NO and an isotopic exchange with ¹⁵NO, similar to that presented in Section 3.2.2, revealed the formation of ¹⁴N¹⁵N di-nitrogen species. This important result was explained as resulting from the isotopic exchange of ¹⁵NO with a ¹⁴NO_x adsorbed species adjacent to another, structurally different nonexchangeable ¹⁴NO_x species. In the presence of H₂, the latter two species are reduced in a coupling mode, leading to ¹⁴N¹⁵N(g) and H₂O. The formation of suggested coadsorbed NO_x species finds support in the literature [27,35,36]. One of the species suggested was nitrosyl (NO⁺) coadsorbed with a nitrate (NO₃⁻) on an adjacent metal cation–oxygen anion site pair on MgO surfaces. In the present case, NO⁺ is suggested to be the exchangeable NO_x species, whereas NO₃⁻ is the nonexchangeable one.

Based on the SSITKA-DRIFTS results (at T = 120°C) presented in Figs. 2a–2c, other IR bands due to adsorbed NO_x did not give a red isotopic shift of the N–O stretching vibrational mode. Although these species were formed under H₂-SCR reaction conditions, they did not participate in the reaction pathways to form N₂ and N₂O. For example, the IR bands at 1370 and 2360 cm⁻¹ reported in Figs. 2a and 2c, respectively, correspond to adsorbed NO₂⁺ on the support (MgO and CeO₂; Table 2), whereas that at 2120 cm⁻¹ corresponds to another kind of inactive nitrosyl (NO^{δ+} and/or NO₂^{δ+}) species on the MgO and/or CeO₂ support (see Table 2). Other inactive adsorbed species identified included chelating nitrite (NO₂⁻) (1370 cm⁻¹; Fig. 2a) and nitritos (1465 cm⁻¹; Fig. 2b) (see Table 2).

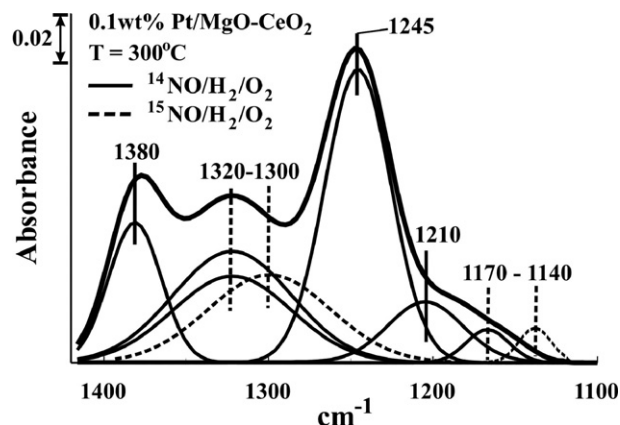


Fig. 3. Deconvolution and curve fitting of SSITKA-DRIFTS spectra recorded at 300 °C in the H₂-SCR of NO over 0.1 wt% Pt/MgO-CeO₂ catalyst in the spectral region 1420–1100 cm⁻¹.

We recently provided strong evidence that reduction of active NO_x formed within a region near the metal–support interface of the present H₂-SCR catalytic system proceeds through an H-spillover process, with Pt providing the H-spilt species [21]. But these H-spilt species cannot diffuse a long distance away from the Pt clusters-support periphery, according to the results of transient DRIFTS-H₂ experiments (see Section 3.1.2). As a result, the structurally similar NO_x species appears to be *active* and *inactive* reaction intermediate. Based on this fact, two IR bands at 1250 cm⁻¹ (Fig. 2a) and 2220 cm⁻¹ (Fig. 2c) were used in the deconvolution and curve-fitting procedures of the IR spectrum obtained under the ¹⁴NO/H₂/O₂ gas mixture.

As the reaction temperature of H₂-SCR was increased to 300 °C, an additional NO_x adsorbed species of different structure appeared to be an *active reaction intermediate* (Fig. 3). The observed IR band shifts (1320 to 1300 cm⁻¹ and 1170 to 1140 cm⁻¹) correspond more closely to the asymmetric (*v*_a) and symmetric (*v*_s) N–O₂ stretch of the *chelating nitrite* (NO₂⁻) species (Table 2). It should be noted that this pair of IR bands, which provided a red isotopic shift (Fig. 3), appears to correspond only to the chelating nitrite species, based on the reported vibrational frequency data of Table 2.

It also is important to note that the bidentate or monodentate nitrate species (1250 and 1560 cm⁻¹, Fig. 2) that appeared to be active species formed at 120 °C on MgO were *not active* at 300 °C, as indicated by the absence of an observable red isotopic shift in that region. On the other hand, *nitrosyl* (NO⁺) *co-adsorbed with a nitrate* (NO₃⁻) species on adjacent metal cation–oxygen anion site pair of the CeO₂ support surface still appeared to be an active reaction intermediate species at 300 °C (IR band red shift from 2220 to 2180 cm⁻¹, not shown). The observed IR bands at 1380/1210 and 1245 cm⁻¹ correspond to *chelating nitrite*, *bidentate*, and/or *monodentate nitrate* species, which are considered *inactive* NO_x intermediates. These species cannot be reached by the H-spilt species from the Pt to the support surface to become reduced, as discussed in more detail later.

Fig. 4 presents IR bands recorded in the 1710–1570 cm⁻¹ range under steady-state H₂-SCR at 120 °C in both isotopic feed compositions. The figure also shows the deconvolution/curve fitting of the IR band recorded under ¹⁴NO/H₂/O₂ into four IR bands (1677, 1640, 1625, 1600 cm⁻¹). The band at 1625 cm⁻¹ is reported to be due to bridged NO species as well as to monodentate or bridged nitrates *formed on Pt* (see Table 2). The latter species is the result of oxidation of Pt either by the presence of gaseous oxygen (cofed with NO) or by the dissociation of adsorbed NO. The IR band at 1640 cm⁻¹ is characteristic of the vibrational bending mode of adsorbed water as well as of bridged NO. The IR band at 1677 cm⁻¹ is suggested to be due to bridged NO on Pt (Table 2), whereas that

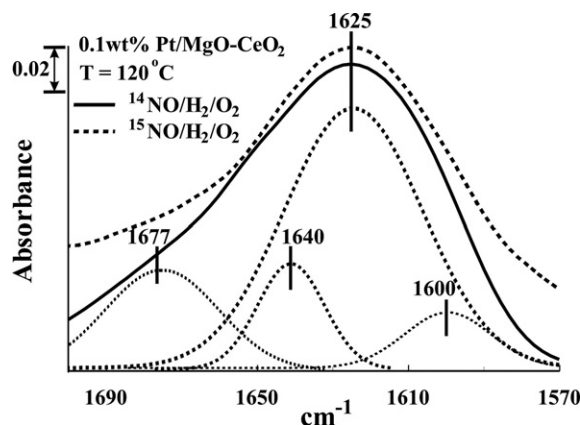


Fig. 4. Deconvolution and curve fitting of SSITKA-DRIFTS spectra recorded at 120 °C in the H₂-SCR of NO over 0.1 wt% Pt/MgO-CeO₂ catalyst in the spectral region 1710–1570 cm⁻¹. Infrared bands at 1677, 1625 and 1600 cm⁻¹ correspond to adsorbed NO_x on Pt (*inactive* NO_x species), while the IR band at 1640 cm⁻¹ to adsorbed water on Pt.

at 1600 cm⁻¹ is attributed to bridged NO or nitrate on Pt. All three IR bands (at 1677, 1625 and 1600 cm⁻¹) probe for the heterogeneity of Pt surface supported on MgO and CeO₂ carriers.

It is very important to note that under the isotopic feed composition of ¹⁵NO/H₂/O₂, *no red isotopic shift* in any of the IR bands reported in Fig. 4 could be observed. Thus, irrespective of some doubts about the true nature of adsorbed NO_x on the Pt surface, the latter species *cannot* be considered as *true active* reaction intermediates. Given the accuracy of the subsequent deconvolution and curve-fitting procedures, we cannot exclude the possibility that a small surface concentration of adsorbed NO_x on Pt that cannot provide a measurable isotopic shift could participate in the reaction path of H₂-SCR. This statement does not alter the main picture of the SSITKA-DRIFTS and SSITKA-MS results (see Section 3.2.1), which provide strong evidence that the active NO_x reaction intermediates are formed mainly on the support close to the Pt–support interface. Similar behavior as shown in Fig. 4 also was seen at a higher reaction temperature (*T* = 300 °C).

Similar SSITKA-DRIFTS experiments (Fig. 1) were performed at other reaction temperatures (*T* = 140 [21] and 150 and 200 °C [this work]). After appropriate spectral band deconvolution and curve-fitting (see Figs. 2 and 3), the following findings were seen:

- In the temperature range of 120–200 °C, *two active* NO_x reaction intermediates were formed: *bidentate or monodentate nitrate* located on the MgO support and *nitrosyl* (NO⁺) *co-adsorbed with a nitrate* (NO₃⁻) species on adjacent metal cation–oxygen anion site pair on the CeO₂ support.
- In the 200–300 °C range, the *bidentate or monodentate nitrate* became *inactive*, whereas *chelating nitrite* (NO₂⁻) appeared to be a *new active* reaction intermediate. *Nitrosyl* (NO⁺) *co-adsorbed with a nitrate* (NO₃⁻) species on adjacent metal cation–oxygen anion site pair of the CeO₂ support also appeared to be an *active* reaction intermediate in the same temperature range.

3.1.2. Reactivity toward hydrogen of adsorbed NO_x formed in H₂-SCR

Fig. 5 presents IR bands in the 1450–1150 (Fig. 5a) and 2300–2150 cm⁻¹ (Fig. 5b) ranges recorded during *transient isothermal reaction in H₂* experiments of adsorbed NO_x formed after steady-state H₂-SCR of NO at 120 °C. DRIFTS spectra were recorded every 1 min under the 10%H₂/He gas mixture used. These experiments were designed to explore whether all or part of the adsorbed NO_x that is identified as an *active* reaction intermediate (see Figs. 2 and 3) and resides on the MgO and CeO₂ supports can be reduced by hydrogen.

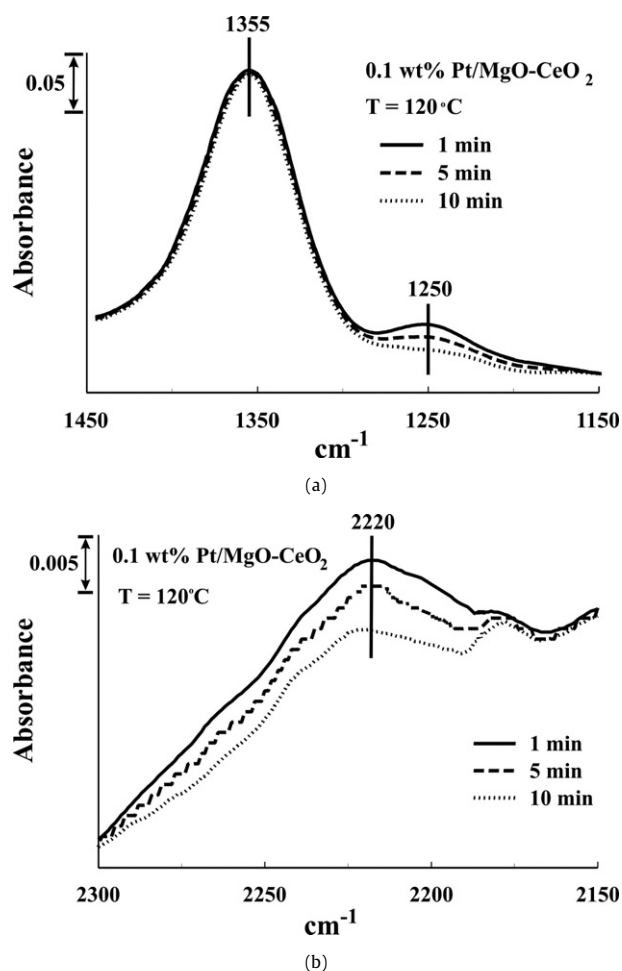
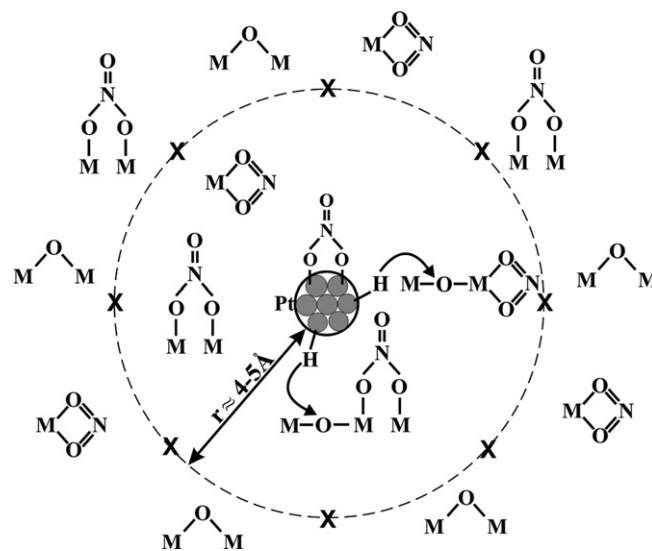


Fig. 5. In situ DRIFTS spectra recorded in the 1450–1150 cm^{-1} (a) and 2300–2150 cm^{-1} (b) range under transient isothermal reaction in H_2 following H_2 -SCR at 120 °C. Spectra recorded after 1, 5 and 10 min in 10% H_2 /He stream are shown.

In the case of *bidentate* or *monodentate nitrate* species (Fig. 5a, IR band at 1250 cm^{-1}), after 10 min on 10% H_2 /He gas stream, no further decrease in the area band (after deconvolution) was obtained. The same result was found in the case of *nitrosyl* (NO^+) *co-adsorbed with a nitrate* (NO_3^-) species on adjacent metal cation–oxygen anion site pair of the CeO_2 support, as shown in Fig. 5b (IR band at 2220 cm^{-1}). On the other hand, the area of the IR band at 1355 cm^{-1} (Fig. 5a) clearly did not change under the isothermal reaction in 10% H_2 /He. This result is consistent with the results shown in Fig. 2a (IR band at 1370 cm^{-1} after deconvolution), where the corresponding NO_x species appeared to be inactive for the H_2 -SCR of NO.

The results of Fig. 5 are very elucidative and important, strongly suggesting that *only a fraction* of the NO_x species that were identified by SSITKA-DRIFTS (Figs. 2 and 3) as *active* and that reside on the support react with H_2 to form mainly N_2 and water [12–15]. This is clearly shown in Fig. 2a for bidentate or monodentate nitrate species, in which the best deconvolution was obtained with a band centered at 1250 cm^{-1} comprising one band that did not shift after the isotopic switch and a second, smaller band at the same position that did shift to 1210 cm^{-1} after the isotopic switch. These results can be explained by considering the fact that the only possible mechanism for reducing the active NO_x formed on the support near the Pt–support interface is the spillover of H species from the Pt surface [21]. But here the H-spilt species apparently were not able to reach the structurally similar NO_x adsorbed



Scheme 1. Hydrogen diffusion on the MgO and CeO_2 support surfaces (M–O–M) is limited to a region (circle in dashed line) of about 4–5 Å radius around the Pt nanoparticles. NO_x reaction intermediates of the H_2 -SCR identified as *active* species by SSITKA-DRIFTS experiments are located within the marked dashed line circle, whereas those located outside of it are considered as *inactive* reaction intermediates.

species located further from the Pt–support interface, as illustrated in Scheme 1.

Based on the concentration ($\mu\text{mol/g}$) of active NO_x reaction intermediates measured by SSITKA-MS (see Section 3.2.1), the Pt mean particle size (1.3 nm), and the average number of M–O pairs per nm^2 (based on MgO and CeO_2 crystallographic data), assuming a hemispherical geometry for the Pt nanoparticles, and considering that for every surface M–O pair ($\text{M}=\text{Ce}^{4+}$, Mg^{2+}) corresponds one active adsorbed NO_x species, it is possible to estimate the radius of the ring around each Pt nanoparticle within which the active NO_x is located. On average, the active NO_x (13.5 $\mu\text{mol/g}$; see Section 3.2.1) were formed within about a 4–5 Å radius around each Pt nanoparticle (see Scheme 1), at most two lattice constants (referred to MgO and CeO_2 supports) away from the Pt–support interface.

Recent quantum chemical calculations (DFT with gradient-corrected functionals) on H surface diffusion on MgO, Pd, and Pd–MgO metal–support boundaries [37] revealed several important properties related to the present study. First, the activation energy for the H atom surface diffusion on Pd is about 4 kcal/mol, with a very significant likelihood of barrier crossing. Second, the energetically favorable location for H atom diffusion on the MgO surface is over the O^{2-} ion. The shape of the energy surface rules out the possibility of an easy migration of the H atom over the MgO surface; however, jumps to the neighboring oxygen sites or by tunneling is a possibility. Third, the transfer of H atoms from Pd to the O site of MgO is energetically favorable, with an excess energy on the order of 0.5 eV (11.5 kcal/mol), with significant rates expected at higher temperatures.

Martin and Duprez [38] studied the isotopic exchange of $\text{D}_2(\text{g})$ and H (–OH groups) on MgO and CeO_2 and other metal oxide surfaces, where surface diffusion coefficients of H were estimated, and also investigated the migration of H from the Rh surface to the support (supported-Rh catalysts). They found that H mobility (surface diffusion coefficient) on MgO and CeO_2 in the 75–200 °C range was significantly greater than that observed on metal oxides of mild Brønsted acidity (e.g., Al_2O_3 and ZrO_2). In the case of MgO and CeO_2 , migration of H on the metal oxide surface could occur without a prerequisite for O–H bond dissociation on the oxide surface at temperatures of 300–400 °C [38]. On the other hand, for

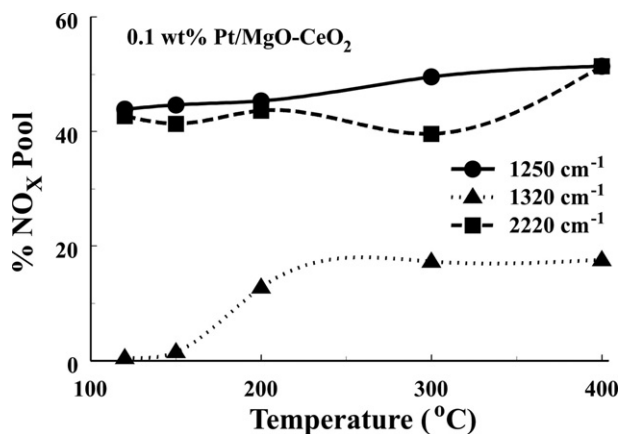


Fig. 6. Percentage (%) of NO_x pool corresponding to bidentate or monodentate nitrate (IR band at 1250 cm⁻¹), chelating nitrite (IR band at 1320 cm⁻¹) and nitrosyl (NO⁺) co-adsorbed with nitrate (NO₃⁻) on adjacent metal cation–oxygen anion site-pair of the CeO₂ support (IR band at 2220 cm⁻¹) that react in 10%H₂/He gas mixture as a function of reaction temperature in the H₂-SCR of NO over the 0.1 wt% Pt/MgO–CeO₂ catalyst.

Al₂O₃ and ZrO₂ (mild acidity), H migration could occur either by the formation of OH₂ intermediate species or by hydrogen jumps, depending on the degree of hydroxylation of the metal oxide surface [38]. For the present H₂-SCR on Pt/MgO–CeO₂, H diffusion on Pt in the 120–160 °C range (partially reduced Pt surface) appeared to be not difficult; however, H migration on the support (MgO and CeO₂) surface will become energetically difficult beyond a distance of about 5 Å from the Pt nanoparticle (see Scheme 1).

The fraction of the NO_x species that were identified as active reaction intermediates (Figs. 2 and 3) and that reacted with hydrogen under the transient isothermal DRIFTS experiments shown in Fig. 5 could be estimated based on the ratio of the integral IR band associated with the given NO_x species after 10 min in 10% H₂/He gas stream to the integral IR band at the start of the experiment (before reaction with the 10%H₂/He gas mixture). Fig. 6 presents the percentage of NO_x pool formed after 30 min of H₂-SCR at a given reaction temperature (120–400 °C) over the 0.1 wt% Pt/MgO–CeO₂ catalyst reacted with hydrogen during 10 min in 10% H₂/He after H₂-SCR (Fig. 5). It can be seen that for bidentate or monodentate nitrate (1250 cm⁻¹) and nitrosyl (NO⁺) coadsorbed with a nitrate (NO₃⁻) species (2220 cm⁻¹), the percentage of active NO_x changed only slightly with reaction temperature. In contrast, chelating nitrites (1320 cm⁻¹) become active at about 200 °C, and their surface concentration accessible to hydrogen reduction remains practically constant at 200–400 °C. These latter results are in harmony with the results of our subsequent SSITKA-MS experiments, in which the concentration (μmol/g) of all active NO_x leading to N₂ was accurately measured.

3.2. Transient mass spectrometry

3.2.1. SSITKA experiments

The surface concentration (μmol/g) and the surface coverage, θ (based on the surface Pt atoms), of the active reaction intermediate NO_x species of the H₂-SCR in the 120–300 °C range was accurately measured by SSITKA-MS [20,21]. Figs. 7 and 8 show transient response curves of the di-nitrogen isotopic ¹⁴N₂ and ¹⁴N¹⁵N species obtained after the switch ¹⁴NO/H₂/O₂ (T, 30 min) → ¹⁵NO/H₂/O₂ (T, t) at 120 and 200 °C, respectively. The results are expressed in terms of the dimensionless concentration Z, which corresponds to the fraction of the ultimate change (giving Z = 0) as a function of time, t. Thus, Z is defined by

$$Z(t) = \frac{(y(t) - y_{\infty})}{(y_0 - y_{\infty})} \quad (1)$$

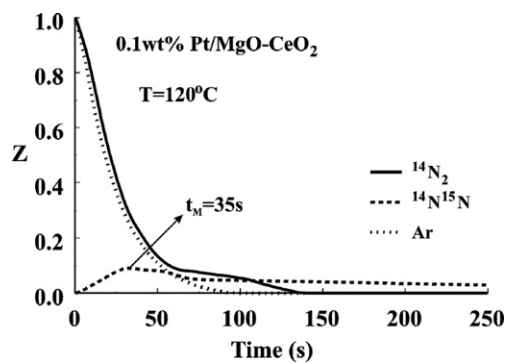


Fig. 7. Transient response curves of ¹⁴N₂, ¹⁴N¹⁵N and Ar obtained during SSITKA-mass spectrometry experiments (¹⁴NO/H₂/O₂/Ar/He → ¹⁵NO/H₂/O₂/He) at 120 °C over the 0.1 wt% Pt/MgO–CeO₂ catalyst.

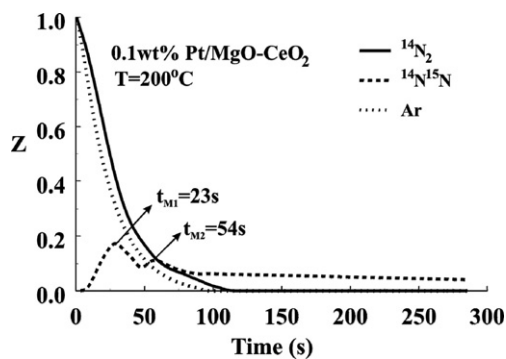


Fig. 8. Transient response curves of ¹⁴N₂, ¹⁴N¹⁵N and Ar obtained during SSITKA-mass spectrometry experiments (¹⁴NO/H₂/O₂/Ar/He → ¹⁵NO/H₂/O₂/He) at 200 °C over the 0.1 wt% Pt/MgO–CeO₂ catalyst.

where the subscripts 0 and ∞ represent the values of y (mole fraction) at t = 0 and long after the isotopic switch (t → ∞). The decay of Ar gas concentration shown in Figs. 7 and 8 was used to monitor the gas phase holdup of the system [20]. The ¹⁴N¹⁵N species is the main one; little ¹⁴N₂ was seen (Figs. 7 and 8), because the amount (μmol/g) of ¹⁴N₂(g) is proportional to the area difference between the Ar and ¹⁴N₂ transient response curves [20]. As the reaction temperature was increased from 120 to 200 °C, a second peak in the ¹⁴N¹⁵N transient response curve developed. This finding reflects the different reduction kinetics of the two active NO_x species present, the nature of which was identified by SSITKA-DRIFTS experiments (see Section 3.1) and was found to depend on reaction temperature. At 120 °C, the transient rate of ¹⁴N¹⁵N formation showed only one peak at t_m = 35 s, whereas two rate maxima appeared at 200 °C (t_m¹ = 23 and t_m² = 54 s; Fig. 8). The latter peaks were seen to shift to lower reaction times at T = 300 °C (t_m¹ = 19 s and t_m² = 45 s).

The concentration of active NO_x that truly participate in the reaction path to form N₂ was estimated by integrating the transient response curves of ¹⁴N¹⁵N and of ¹⁴N₂ with respect to the Ar curve (Figs. 7 and 8). Fig. 9a presents the results obtained in terms of μmol/g of catalyst or surface coverage (θ) as a function of reaction temperature. The surface coverage θ is referred to the exposed surface Pt atoms (μmolPt_s/g). Values of θ greater than unity indicate that at least part of the estimated active NO_x cannot reside on Pt. For the present catalytic system, according to the DRIFTS-SSITKA results (see Section 3.1) all of the active NO_x reside on the support (vicinity of Pt–support interface, Scheme 1). Fig. 9a illustrates that in the 120–300 °C range θ takes values significantly larger than unity, between 2.3 and 2.7 (θ_{max} = 2.7 at 140 °C). On the other hand, it should be noted that these differences are small. There-

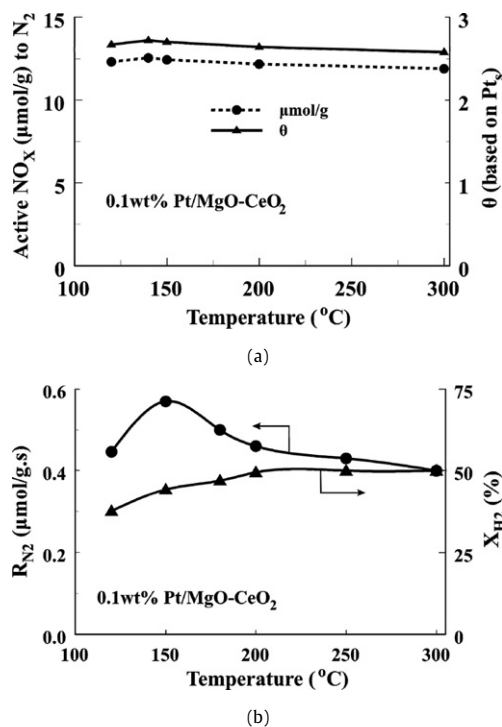


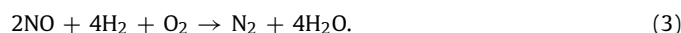
Fig. 9. (a) Concentration (μmol/g) and surface coverage (θ) of active NO_x that lead to N₂ formation as a function of reaction temperature in H₂-SCR estimated from SSITKA–mass spectrometry experiments performed over the 0.1 wt% Pt/MgO–CeO₂ catalyst. (b) Kinetic rate (μmol/g.s) of N₂ formation and H₂ conversion (X_{H_2} , %) as a function of reaction temperature during steady state H₂-SCR of NO.

fore, the concentration of active NO_x stays practically constant in the 120–300 °C range.

Fig. 9b presents the intrinsic kinetic rate (μmol/g.s) of N₂ formation as a function of reaction temperature estimated under steady-state reaction conditions in the ¹⁴NO/H₂/O₂ feed gas mixture, before the isotopic switch to the equivalent ¹⁵NO/H₂/O₂ gas mixture was made (Figs. 7 and 8). The figure also shows the corresponding H₂ conversion versus the reaction temperature. It can be seen that the kinetic rate of H₂-SCR passed through a maximum in a temperature range where the conversion of H₂ was <40%. The volcano-type behavior of the kinetic reaction rate (Fig. 9b) was similar to that obtained for the NO conversion versus reaction temperature reported in previous work [12–14]. It also should be noted that the high values of H₂ conversion were strictly related to its combustion to water, and only a small part of H₂ was used for the conversion of NO into N₂ according to the following reactions:



and



For example, for a 10% NO conversion ($y_{NO}^f = 2500$ ppm) the equivalent H₂ conversion ($y_{H_2}^f = 10,000$ ppm) is only 5% (neglecting small changes in the total molar flow rate of the reaction mixture), compared with the estimated values of >30% (Fig. 9b).

According to the results shown in Figs. 9a and 9b, the appearance of a maximum in the profile of kinetic rate of N₂ formation versus the reaction temperature cannot be attributed to a compensatory increase in the rate constant with increasing reaction temperature and a simultaneous decrease in the surface concentration of active NO_x that led to N₂ formation. Obviously, other intrinsic kinetic factors are responsible for the volcano-type behavior of the reaction rate versus temperature.

As discussed earlier, the surface diffusion of atomic H on the Pt surface toward the metal–support interface should be considered an important step in the present H₂-SCR on Pt/MgO–CeO₂ catalyst. The energy barrier for this surface diffusion step would be expected to be controlled by the surface coverage of other coadsorbed species and the electronic structure of Pt surface atoms under H₂-SCR reaction conditions. In addition, the rate of this surface diffusion step would be expected to be proportional to the surface coverage of atomic H on Pt. Thus, it is reasonable to suggest that an increase in the reaction temperature in the 100–200 °C range would modify some or all of the values of these important kinetic parameters so as to create a maximum in the rate. To identify which of these kinetic parameters most affects the rate of H diffusion on the Pt surface is a difficult but challenging task. Theoretical studies (e.g., DFT calculations) would seem to be a very efficient approach to exploring this issue, because estimating the surface coverage of H, θ_H , of inactive NO_x and adsorbed oxygen, θ_O , on the Pt surface is very difficult under H₂-SCR of NO reaction conditions. This latter parameter seems to play an important role, because the Pt surface over the 0.5 wt% Pt/MgO–CeO₂ catalyst is largely oxidized [17]. In fact, catalytic studies performed on the present Pt/MgO–CeO₂ system with NO/H₂ and NO/H₂/O₂ feed gas mixtures revealed that similar integral rates (or NO conversions) were achieved at 100–160 °C, whereas at higher temperatures the integral rate or NO conversion under the presence of 5%O₂ in the feed of NO/H₂ was significantly reduced (Fig. 6a, Ref. [13]).

It is reasonable to suggest that on the present supported-Pt catalytic system, the stability of Pt–O bonds at temperatures above 160 °C and in the presence of small hydrogen concentrations in the gas phase could be a main reason for the observed maximum in the profile of NO conversion versus reaction temperature [12–14]. On the other hand, in the presence of a sufficiently high hydrogen concentration in the gas phase, the kinetic rate of reaction (although going through a maximum at $T < 160$ °C) demonstrates similar values at low (120 °C) and high (300 °C) reaction temperatures (Fig. 9b). This result implies that reduction of surface PtO_x at $T > 160$ °C cannot be considered a slow reaction step, allowing hydrogen dissociation and surface diffusion of atomic H to proceed without difficulty on the Pt surface. It was recently reported [39] that the oxidation of NO into NO₂ on Pt/Al₂O₃ catalyst is largely favored on large Pt particles, with a fourfold increase in the rate at 300 °C achieved by increasing the Pt particle size from 2.4 to 7.0 nm. Those authors suggested that the lower rates of NO oxidation resulted from the stronger Pt–O bonds formed on the small Pt particles. Considering the fact that NO₂ formation could be an important intermediate for the present catalytic system [21], Pt–O stability behavior with reaction temperature also appears to be an important parameter in the H₂-SCR of NO.

3.2.2. H₂-TPSR after H₂-SCR and ¹⁵NO isotopic exchange

Fig. 10 presents transient response curves of ¹⁴NO and ¹⁴N¹⁵N gaseous species obtained under H₂-TPSR (10%H₂/He flow) over the 0.1 wt% Pt/MgO–CeO₂ catalyst according to the experimental sequence described in Table 1 (experiment B). In the case of H₂-SCR at 120 °C (Fig. 10a), a broad ¹⁴NO desorption response curve comprising two distinct peaks was observed at 30–250 °C, along with a ¹⁴N¹⁵N peak centered at 115 °C with a small shoulder at the rising part of it. The formation of ¹⁴N¹⁵N(g) can be explained by considering that two adjacent adsorbed NO_x species formed under the ¹⁴NO/H₂/O₂ reaction, one of which was exchanged with gaseous ¹⁵NO (under the ¹⁵NO/He treatment of the catalyst), were reduced in a coupling mode to eventually form di-nitrogen ¹⁴N¹⁵N species. We first suggested this phenomenon in a previous report [21], and we have confirmed it in the present study for other H₂-SCR reaction temperatures (Fig. 10). Earlier, we suggested that the two NO_x species participating in the formation of ¹⁴N¹⁵N (Fig. 10) are the

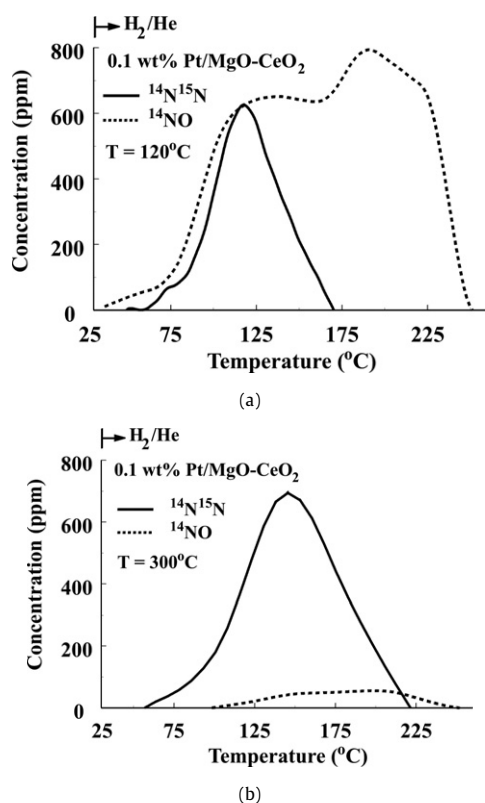


Fig. 10. Transient response curves of ^{14}NO and $^{14}\text{N}^{15}\text{N}$ gaseous species obtained during H_2 -TPSR (10% H_2 /He flow) according to the experimental sequence described in Table 1 (Expt. B) over the 0.1 wt% Pt/MgO–CeO₂ catalyst. (a) $T = 120^\circ\text{C}$, (b) $T = 300^\circ\text{C}$; $Q_{\text{H}_2/\text{He}} = 30 \text{ N mL/min}$; $W = 0.15 \text{ g (Pt/MgO–CeO}_2\text{)}$.

NO^+ (nitrosyl) and NO_3^- (nitrate) co-adsorbed on adjacent metal cation–oxygen anion site pair of the CeO₂ support surface (see Section 3.1.1). The exchangeable adsorbed $^{14}\text{NO}_x$ species with gaseous ^{15}NO is that of $^{14}\text{NO}^+$ (nitrosyl), whereas the nonexchangeable one is that of $^{14}\text{NO}_3^-$ (nitrate).

An alternative explanation for the appearance of $^{14}\text{N}^{15}\text{N}$ response curve in the H_2 -TPSR of Fig. 10 could be that the exchangeable $^{14}\text{NO}_x$ species (labeled $^{15}\text{NO}_x$) diffused toward a nonexchangeable species (labeled $^{14}\text{NO}_x$) during H_2 -TPSR, with simultaneous reduction/coupling to form $^{14}\text{N}^{15}\text{N}(\text{g})$ and H_2O . This explanation is difficult to accept, however, because the two active NO_x species identified for the present H_2 -SCR catalytic system were not located on the same solid surface (see Section 3.1). Earlier, we clearly demonstrated that the first active NO_x species is located in the vicinity of the Pt–MgO interface, with the other located in the vicinity of the Pt–CeO₂ interface (see Scheme 1). Therefore, diffusion of the first NO_x species from ceria particles to reach the second NO_x species on MgO particles, or vice versa, to become reduced in the presence of hydrogen is much less likely than the coupling/reduction of *two adjacent* NO_x on the same surface, as suggested previously.

As the reaction temperature of H_2 -SCR was increased to 300°C , the features of the corresponding traces of $^{14}\text{N}^{15}\text{N}$ and ^{14}NO changed (Fig. 10b). The $^{14}\text{N}^{15}\text{N}$ transient response curve was similar in shape to that obtained at $T = 120^\circ\text{C}$ (Fig. 10a), but its maximum shifted to a higher temperature ($T_M = 140^\circ\text{C}$), and its concentration was doubled ($6.6 \mu\text{mol/g}$ at 300°C vs $3.2 \mu\text{mol/g}$ at 120°C). These findings imply that some factors were influencing the kinetics of reduction/coupling of *nitrosyl* (NO^+) *coadsorbed with a nitrate* (NO_3^-) species to form $^{14}\text{N}^{15}\text{N}$, and also that the shape and amount of desorbed ^{14}NO were significantly influenced by the reaction temperature in H_2 -SCR (compare Figs. 10a and 10b). The

Table 3

Concentration ($\mu\text{mol/g}$) of N-containing species formed during H_2 -TPSR according to the following experimental sequence of steps: $^{14}\text{NO}/\text{H}_2/\text{O}_2/\text{He}$ (30 min, T) \rightarrow $^{15}\text{NO}/\text{He}$ (15 min, T) \rightarrow cool quickly to room T in $^{15}\text{NO}/\text{He}$ \rightarrow He (5 min) \rightarrow H_2 -TPSR (10% H_2/He)

T ($^\circ\text{C}$)	^{14}NO ($\mu\text{mol/g}$)	$^{14}\text{N}^{15}\text{N}$ ($\mu\text{mol/g}$)	Total NO_x ($\mu\text{mol/g}$)
120	7.8	3.2	14.2
150	6.8	3.8	14.4
200	3.3	4.9	13.1
300	0.7	6.6	13.9
400	0.2	6.7	13.2

latter finding is related to the fact that the chemical structure of one of the active NO_x of H_2 -SCR formed on MgO support changed from bidentate or monodentate nitrate (NO_3^-) to chelating nitrite (NO_2^-) (see Section 3.1).

Table 3 reports the concentrations ($\mu\text{mol/g}$) of $^{14}\text{N}^{15}\text{N}$ and ^{14}NO species formed under H_2 -TPSR (Fig. 10) as a function of reaction temperature (H_2 -SCR). The table clearly shows that the amount of $^{14}\text{N}^{15}\text{N}(\text{g})$ increased monotonically with reaction temperature, whereas the opposite was true for the nonexchangeable NO_x species [$^{14}\text{NO}(\text{g})$ in Fig. 10]. On the other hand, the total concentration of NO_x changed only slightly with reaction temperature, in accordance with the SSITKA-MS findings (Fig. 9). All of these features seem reasonable given the differences in the chemical structure of active NO_x , and thus its thermal stability and reduction kinetics, with changes in reaction temperature.

4. Conclusion

The following conclusions can be derived from the results of the present work on H_2 -SCR of NO over a novel 0.1 wt% Pt/MgO–CeO₂ catalyst [15]:

- Two active NO_x intermediate species were identified by SSITKA-DRIFTS in the nitrogen-reaction path toward N_2 formation, one in the vicinity of the Pt–CeO₂ support interface (*nitrosyl* [NO^+] *coadsorbed with nitrate* [NO_3^-] on adjacent Ce^{4+} -oxygen anion site pair), and the other located in the vicinity of the Pt–MgO support interface. The chemical structure of the latter species was found to depend on reaction temperature. Below 200°C , the second active NO_x has the structure of *bidentate or monodentate nitrate* (NO_3^-), whereas above 200°C , it has the structure of *chelating nitrite* (NO_2^-).
- The concentration ($\mu\text{mol/g}$) of active NO_x reaction intermediates leading to N_2 formation was practically independent of reaction temperature (120 – 300°C) and significantly larger than 1 equivalent monolayer of surface Pt ($\theta_{\text{NO}_x} = 2.4$ – 2.6). This result cannot explain the volcano-type behavior of catalytic activity (kinetic rate and NO conversion) versus reaction temperature observed in the present work and also reported previously [12–14].
- Surface diffusion of H species on the MgO and CeO₂ support surfaces (the former spilt over from the Pt metal to the support surface) is limited within a region of about 4–5 Å around the Pt nanoparticles. This is the main reason why not all NO_x formed on the MgO and CeO₂ support surfaces under H_2 -SCR conditions became active reaction intermediates.

References

- [1] H. Bosch, F. Janssen, *Catal. Today* 2 (1988) 369.
- [2] F. Nakajima, I. Hamada, *Catal. Today* 29 (1996) 109.
- [3] Shell International Research Maatschappij, Eur. Patent 0 217 446.
- [4] E. García-Bordejé, J.L. Pinilla, M.J. Lázaro, R. Moliner, J.L.G. Fierro, *J. Catal.* 233 (2005) 166.
- [5] L. Singoredjo, R. Korver, F. Kapteijn, J.A. Moulijn, *Appl. Catal. B: Environ.* 1 (1992) 297.

- [6] B.W.L. Jang, J.J. Spivey, M.C. Kung, H.H. Kung, *Energy Fuels* 11 (1997) 299.
- [7] C.J.G. van der Grift, A.F. Woldhuis, O.L. Maaskant, *Catal. Today* 27 (1996) 23.
- [8] G. Ertl, H. Knözinger, J. Weitkamp, in: *Handbook of Heterogeneous Catalysis*, VCH, Weinheim, Germany, 1997, p. 1633.
- [9] H. Gutberlet, B. Schallert, *Catal. Today* 16 (1993) 207.
- [10] C.N. Costa, V.C. Belessi, V.N. Stathopoulos, A.M. Efstathiou, *J. Catal.* 197 (2001) 350.
- [11] C.N. Costa, P.G. Savva, C. Andronikou, P. Lambrou, K. Polychronopoulou, V.C. Belessi, V.N. Stathopoulos, P.J. Pomonis, A.M. Efstathiou, *J. Catal.* 209 (2002) 456.
- [12] C.N. Costa, A.M. Efstathiou, *Environ. Chem. Lett.* 2 (2004) 55.
- [13] C.N. Costa, A.M. Efstathiou, *Appl. Catal. B: Environ.* 72 (2007) 240, and references therein.
- [14] C.N. Costa, P.G. Savva, J.L.G. Fierro, A.M. Efstathiou, *Appl. Catal. B: Environ.* 75 (2007) 149, and references therein.
- [15] A.M. Efstathiou, C.N. Costa, J.L.G. Fierro, US Patent 7, 105, 137 B2 (2006); Spanish Patent ES 2 192 985 B1 (2005); Eur. Patent Application No. 03704721, to be granted.
- [16] K. Balakrishnan, R.D. Gonzalez, *J. Catal.* 144 (1993) 395.
- [17] C.N. Costa, Ph.D. thesis, University of Cyprus, 2003.
- [18] C.N. Costa, T. Anastasiadou, A.M. Efstathiou, *J. Catal.* 194 (2000) 250.
- [19] C.N. Costa, S.Y. Christou, G. Georgiou, A.M. Efstathiou, *J. Catal.* 219 (2003) 259.
- [20] A.M. Efstathiou, X.E. Verykios, *Appl. Catal. A: Gen.* 151 (1997) 109.
- [21] C.N. Costa, A.M. Efstathiou, *J. Phys. Chem. C* 111 (2007) 3010, and references therein.
- [22] B.C. Smith, *Fundamentals of Fourier Transform Infrared Spectroscopy*, CRC Press, 1996.
- [23] B. Klingenberg, M.A. Vannice, *Appl. Catal. B: Environ.* 21 (1999) 19.
- [24] K.I. Hadjiivanov, *Catal. Rev.—Sci. Eng.* 42 (2000) 71, and references therein.
- [25] J. Müslehiddinoğlu, M.A. Vannice, *J. Catal.* 217 (2003) 442.
- [26] C.N. Costa, A.M. Efstathiou, *J. Phys. Chem. B* 108 (2004) 2620.
- [27] K. Hajjiivanov, V. Bushev, M. Kantcheva, D. Klissurski, *Langmuir* 10 (1994) 464.
- [28] S.J. Huang, A.B. Walters, M.A. Vannice, *J. Catal.* 192 (2000) 29.
- [29] J.W. London, A.T. Bell, *J. Catal.* 31 (1973) 32.
- [30] A. Bourane, O. Dulaurent, S. Salasc, C. Sarda, C. Bouly, D. Bianchi, *J. Catal.* 204 (2001) 77, and references therein.
- [31] B.A. Morrow, R.A. McFarlane, L.E. Moran, *J. Phys. Chem.* 89 (1985) 77.
- [32] J.A. Rodriguez, T. Jirsak, *J. Chem. Phys.* 112 (2000) 9929.
- [33] K. Nakamoto, *Infrared and Raman Spectra of Inorganic and Coordination Compounds*, fourth ed., Wiley, New York, 1986.
- [34] M. Machida, S. Ikeda, *J. Catal.* 227 (2004) 53.
- [35] W.F. Schneider, K.C. Hass, M. Miletic, J.L. Gland, *J. Phys. Chem. B* 106 (2002) 7405.
- [36] M. Miletic, J.L. Gland, K.C. Hass, W.F. Schneider, *Surf. Sci.* 546 (2003) 75.
- [37] W.M. Bartczak, J. Stawowska, *Mater. Sci.—Poland* 24 (2006) 421.
- [38] D. Martin, D. Duprez, *J. Phys. Chem. B* 101 (1997) 4428.
- [39] S.S. Mulla, N. Chen, L. Cumaranatunge, G.E. Blau, D.Y. Zemlyanov, W.N. Delgass, W.S. Epling, F.H. Ribeiro, *J. Catal.* 241 (2006) 389.